Analytical Scaling of Trap-Limited Current in 2-D Ultrathin Dielectrics

Chun Yun Kee, Yee Sin Ang, *Member, IEEE*, Er-Ping Li, *Fellow, IEEE*, and L. K. Ang, *Fellow, IEEE*

***Abstract*— For charge injection from an electrode into a trap-filled dielectric slab, its current–voltage (*I–V*) characteristics are governed by the Mark–Helfrich (MH) law. By matching the experimentally measured *I–V* characteristics to a right *I–V* model, one can characterize the microscopic properties of the dielectric like its carrier mobility and traps distribution. The original MH law was developed for a bulk solid and may not be valid for modern ultrathin dielectrics used in 2-D electronics. Here, we revise the MH law for an ultrathin trap-filled dielectric of length *L* biased with a voltage of *V*. Our model suggests a new scaling of the current line density: $J_{2\text{-D}} \propto [(V/\alpha L)\exp(-(\beta l/l+1))]^{l+1}$, where $\alpha = (2.8, 2.03)$ and $\beta = (1.02, 0.94)$ are numerical values for two different geometrical (edge, strip) contacts, respectively. Using this 2-D ultrathin MH law, we demonstrate that the estimated carrier mobility can be significantly different from the traditional MH law. Under the same material properties, our model also highlights that strip contact geometry will always lead to a larger current flow than edge contact geometry. Thus, the developed model should be useful for the characterization of the ultrathin dielectrics used in 2-D materials-based electronics, organic semiconductors, and thin-film electronics.**

***Index Terms*— Dielectrics, mobility, thin films, trap-limited current, traps.**

I. Introduction

CHARGE injection from an electrode into a dielectric material at the high-voltage regime is known as the space–charge-limited current (SCLC) conduction [1]. By measuring the current–voltage (I–V) characteristics, the carrier mobility [2], trap characteristics [3], [4], and the underlying charge transport mechanisms [5], [6], [7] can be determined by fitting the experimental measurement with the correct SCLC models. For a trap-free bulk dielectric in a parallel-plate diode, the SCLC is governed by the Mott–Gurney (MG) law [8]

$$J_{\text{MG}} = \frac{9}{8}\,\epsilon\,\mu\frac{V^2}{L^3} \tag{1}$$

where J is the current density, V is the applied bias voltage, L is the length of the dielectrics between two electrodes, ϵ is the permittivity of the dielectric material, and μ is the carrier mobility. This MG law is the solid-state counterpart to the Child–Langmuir (CL) law for vacuum diode [9], [10]: $J_{\text{CL}} \propto V^{3/2}/L^2$. Studies of SCLC can be found in recent review papers [5], [11]. Recently revised models of MG law include finite emission [12], [13], solids with nanocontacts [14], nanowires [15], quantum effects [16], transition models [17], and capacitance formulation [18].

Extending the MG law for a dielectric into the *ultrathin* film configuration [19] in the limit of vanishing thickness of the dielectric ($D \ll L$), the current line density $\mathcal{J}$ is

$$\mathcal{J}_{\text{2-D}}[\text{MG}] = \zeta_{\text{2-D}}\epsilon\mu\left(\frac{V}{L}\right)^2 \tag{2}$$

where $\zeta_{\text{2-D}}$ is a parameter depending on contact geometry, numerically determined to be 0.57, 0.7, and 1.0 for three different contact configurations, namely edge, coplanar strip, and perpendicular plane contact, respectively. Here, the I–V scaling remains $\mathcal{J}_{\text{2-D}} \propto V^2$, but the current–length scaling is modified to a *non-MG* form of $\mathcal{J}_{\text{2-D}} \propto L^{-2}$. Compared with the drift-diffusion current transport simulation of a dielectric thin-film diode [19], (2) is found to exhibit good agreement with the simulated I–V characteristics, while the bulk MG law (1) exhibits more than one order of magnitude in error.

Traps in dielectrics are common and unavoidable in organic semiconductor devices [20], [21], [22], [23], [24], [25] and oxide dielectric breakdown [26], [27]. For a dielectric with an exponential trap distribution, the corresponding SCLC model is known as the Mark–Helfrich (MH) law [28]

$$J_{\text{MH}} = N_0\mu e^{1-l}\left(\frac{\epsilon}{N_t}\frac{l}{l+1}\right)^l\left(\frac{2l+1}{l+1}\right)^{l+1}\frac{V^{l+1}}{L^{2l+1}} \tag{3}$$

where e is the electron charge, N_0 is the effective density of states at the conduction band edge, N_t is the total trap density, and $l \equiv T_c/T \geq 1$, with T is the temperature and T_c is a parameter characterizing the exponential spread in the energy of the traps. Note that (3) has a strong dependence of l and very large values of l has been reported [24], [25], [29], [30], [31], [32]. At $l = 1$, the MH law recovers the same scaling of V^2/L^3 like the MG law. For 2-D materials with unconventional *nonparabolic* energy dispersion, the MH law is revised [33]

Manuscript received 17 September 2022; revised 11 November 2022; accepted 12 November 2022. Date of publication 24 November 2022; date of current version 24 March 2023. This work was supported by the Agency for Science, Technology and Research (A*STAR) Advanced Manufacturing and Engineering (AME) Independent Research Grant (IRG) under Grant A2083c0057. The work of Yee Sin Ang was supported by the Singapore Ministry of Education Academic Research Fund (AcRF) Tier 2 under Grant MOE-T2EP50221-0019. The work of Er-Ping Li was supported by the Singapore University of Technology and Design (SUTD)-Zhejiang University (ZJU) Visiting Professor under Grant VP 201303. The review of this article was arranged by Editor M. Lanza. *(Corresponding authors: Yee Sin Ang; L. K. Ang.)*

Chun Yun Kee, Yee Sin Ang, and L. K. Ang are with Science, Mathematics and Technology, Singapore University of Technology and Design, Singapore 487372 (e-mail: chunyun_kee@sutd.edu.sg; yeesin_ang@sutd.edu.sg; ricky_ang@sutd.edu.sg).

Er-Ping Li is with the College of Information Science and Electronic Engineering, Zhejiang University, Hangzhou 310027, China (e-mail: liep@zju.edu.cn).

Color versions of one or more figures in this article are available at https://doi.org/10.1109/TED.2022.3222279.

Digital Object Identifier 10.1109/TED.2022.3222279

with a scaling of $J \propto (V/L)^a$, where a varies continuously from $l/2+1$ to $l+1$ depending on the properties of the 2-D Dirac based materials. Another model to study the trap-limited SCLC in a porous dielectric has been reported to show the different L-scaling [34].

In comparison to the ultrathin MG law [19], to our best knowledge, there is no such ultrathin model for the MH law. In this article, we construct a semianalytical model to calculate the trap-limited current line density for a 2-D ultrathin dielectric that can be useful for van der Waals (vdW) heterostructures-based electronics and optoelectronics [26], [35], [36], [37], [38], [39], [40], [41]. Considering traps that follow an exponential energy distribution, our model provides a scaling of:

$$\mathcal{J}_{\text{2-D}} \propto \left[\frac{V/L}{\lambda_l}\right]^{l+1} = \left[\frac{V}{\alpha L}\exp\left(-\frac{\beta l}{l+1}\right)\right]^{l+1} \tag{4}$$

where α and β are constants depending on the contact geometry. For two representative geometries of *edge* and *strip* contacts (see Fig. 1), we have $\alpha = 2.8, 2.03$ and $\beta = 1.02, 0.94$, respectively. Here, $\lambda_l = \alpha \times \exp[\beta l/(1+l)]$ is a geometric-dependent parameter, which is verified numerically from $l = 1$ to 10 as shown in Fig. 3.

In the remainder of the article, we first present the derivation of scaling relation, followed by the formulation of the charge transport governing equations for an ultrathin dielectric with edge and strip contacts. Evaluating the prefactor requires solving the charge transport governing equations to obtain the l-dependent parameter λ_l. The numerical scheme for solving the governing integral equations is elaborated in Section III. Upon solving the charge transport equations, λ_l for an ultrathin dielectric with edge and strip contacts are evaluated and shown to be well approximated by an empirical formula that leads to the scaling in (4). Lastly, we examine the differences of carrier mobility estimated between (3) and (4) and emphasize our model is more suitable for ultrathin dielectronics. Thus, our model provides a simple analytical tool to characterize the mobility and trap properties of 2-D ultrathin trap-filled dielectrics, which plays an important role in emerging fields such as neuromorphic computing [42], [43], [44], [45] and other 2-D-materials-based electronics [46], [47], [48], [49], [50], [51].

II. MH Law for Ultrathin Dielectrics

A. Scaling of the Trap-Limited Current Line Density

A diagram of an ultrathin dielectric is shown in Fig. 1 with two contact geometries, edge and strip. The dielectric is invariant in the z-direction and lying in the xz-plane with length, thickness, and width of L, D, and W, respectively. In the presence of traps that follow an exponential energy distribution [28], the free and trapped carrier densities are related by

$$n_f(x) = \frac{N_0}{N_t^l} n_s^l \equiv C_l n_s^l \tag{5}$$

where $n_f(x)$ is the free carrier density, $n_s(x)$ is the trapped carrier density, N_0 is the effective density of states at the conduction-band edge, N_t is the trap density, and $l \equiv T_c/T \leq 1$, where T_c is a characteristic temperature representing the exponential spread in energy of the traps. The current continuity equation within the ultrathin dielectric is written as

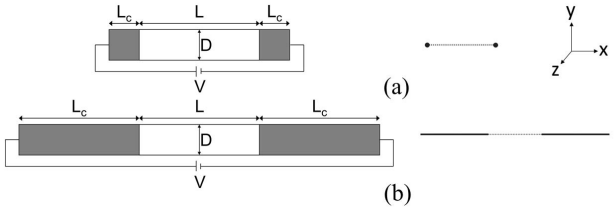

Fig. 1. Ultrathin dielectrics is lying in the *xz*-plane with different contact geometries (shaded). The length, thickness, and width of the dielectric are *L*, *D*, and *W* in *x*-, *y*-, *z*-direction, respectively. The dielectric is invariant in the *z*-direction and connected to a pair of symmetric contact of length, L_c. (a) For edge contact, L_c is comparable to *D* and the two contacts reduce to two points in the limit of $D \to 0$. (b) For strip contact, L_c is comparable to *L* and the two contacts reduce to two lines extended to infinity in the limit of $D \to 0$. With dashed line representing the dielectric length *L*, the corresponding geometrical models in the limit of $D \to 0$ are shown on the right.

$$\mathcal{J} = e\mu n_f(x) E_x(x) = e\mu C_l n_s^l(x) E_x(x) \tag{6}$$

where E_x is the x component of the electric field in the ultrathin dielectric. Rewriting the electric field as

$$E_x(x) = \frac{\mathcal{J}}{e\mu C_l n_s^l(x)} \tag{7}$$

and considering a normalization scheme similar to the prior paper [19], the voltage across the dielectric is

$$V = \int_0^L E_x(x) = \frac{JL}{e\mu C_l}\left(\frac{2e^2\mu C_l}{J\epsilon}\right)^{\frac{l}{l+1}} \int_0^1 \frac{d\xi}{v_s^l(\xi)} \tag{8}$$

with

$$\xi = \frac{x}{L}, \quad v_s(\xi) = \left(\frac{2e^2\mu C_l}{J\epsilon}\right)^{\frac{1}{l+1}} n_s(\xi).$$

With a defined parameter λ_l given by

$$\lambda_l \equiv \int_0^1 d\xi / v_s^l(\xi). \tag{9}$$

The current line density becomes

$$\mathcal{J} = C_l \mu e^{1-l}\left(\frac{\epsilon}{2}\right)^l \left(\frac{V}{\lambda_l L}\right)^{l+1}. \tag{10}$$

Here, λ_l is a l-dependent parameter for a given trap characteristic and contact geometry of the ultrathin dielectric. To evaluate λ_l, the normalized surface charge concentration, v_s, associated with different contact geometries is required.

B. Ultrathin Dielectrics With Edge Contact

A diagram of the ultrathin dielectric with edge contact geometry (left) is shown in Fig. 1(a) with a schematic geometry in the limit of vanishing thickness ($D \ll L$) shown on the right. The dielectric is connected to a pair of symmetric contact with length, L_c, comparable to dielectric thickness D. For $D \ll L$, with the consideration of $D \to 0$ and $L_c \to 0$, the contacts become two conducting filaments and are represented

by two points connected to the dielectric (dashed line) in the xy-plane. The charge and potential distribution within the dielectric are governed by the Poisson equation satisfying the boundary conditions at the electrodes based on (7). Based on the Green's function approach [19], we consider that the charge carriers only reside within the dielectric and focus on the electric field along the dielectric ($y = 0$)

$$G(\xi, \xi') = -\frac{1}{2\pi} \ln L|\xi - \xi'| \tag{11}$$

where

$$\xi = \frac{x}{L}, \quad \xi' = \frac{x'}{L}.$$

The electric potential ϕ is obtained by integrating Green's function over the surface charge concentration along the dielectric (x-direction). With $E_x = -d\phi/dx$, the electric field is given by

$$E_x(\xi) = \frac{2e}{\epsilon(1-\xi)} \int_0^1 \frac{1-\xi'}{\xi - \xi'} n_s(\xi') d\xi'. \tag{12}$$

Here, only the key steps are highlighted, the details of the derivation can be found in the prior work [19]. Combining (7) and (12), the term v_s for the edge contact geometry can be solved from the following normalized singular integral equation:

$$\frac{v_s^l(\xi)}{1-\xi} \int_0^1 \frac{1-\xi'}{\xi - \xi'} v_s(\xi') d\xi' = 1. \tag{13}$$

C. Ultrathin Dielectrics With Strip Contact

A diagram of the ultrathin dielectric with strip contact geometry (left) is shown in Fig. 1(b) with a schematic geometry in the limit of vanishing thickness ($D \ll L$) shown on the right. The dielectric is connected to a pair of symmetric contact of length L_c, comparable to the dielectric length of L. For $D \ll L$, with the consideration of $D \to 0$ and $L_c \to \infty$, each contact becomes a conducting plane coplanar to the dielectric and is represented by line segment (extended to infinity) connected to the dielectric (dashed line) in the xy-plane. Similarly, the corresponding Green's function is

$$G(\xi, \xi') = \frac{1}{2\pi} \text{Re} \ln\left(\frac{\sin[(\theta + \theta')/2]}{\sin[(\theta + \theta')/2]}\right) \tag{14}$$

where

$$\xi = \frac{2x - L}{L}, \quad \theta = \arccos(\xi)$$
$$\xi' = \frac{2x' - L}{L}, \quad \theta' = \arccos(\xi').$$

Note the coordinate system for edge and strip contact geometries are normalized to different intervals of [0, 1] and [−1, 1], respectively, for the convenience of applying Green's function. This notation will be assumed throughout this article unless otherwise stated. After obtaining the electric potential by integrating Green's function over the surface charge concentration along the dielectric and differentiating the potential, the electric field is

$$E_x(\xi) = \frac{2}{\sqrt{1-\xi^2}} \left[\frac{e}{\epsilon} \int_{-1}^1 \frac{\sqrt{1-\xi'^2}}{\xi - \xi'} n_s(\xi') d\xi' + \frac{V}{\pi L}\right]. \tag{15}$$

Similarly, combining (7), (8), and (15), v_s for the strip contact geometry is governed by

$$\frac{v_s^l(\xi)}{\sqrt{1-\xi^2}} \int_{-1}^1 \left[\frac{\sqrt{1-\xi'^2}}{\xi - \xi'} v_s(\xi') + \frac{1}{\pi v_s^l(\xi')}\right] d\xi' = 1. \tag{16}$$

III. Numerical Methods

The resulting singular integral equations, (13) and (16) are solved numerically to obtain the λ_l and hence the prefactor by evaluating $\lambda_l^{-(l+1)}$. It is not trivial to solve the singular integral equation numerically. We first attempt to seek an approximated v_s in terms of the Chebyshev polynomials due to the convenient analytic formula [52] for evaluating the singular integral involved in (13) and (16). Note for large values of l, the convergence of the solutions requires increasingly more terms leading to longer computational time due to the nature of the hypersingular kernel in the equation. There are advanced techniques [53] that may circumvent this issue but they will involve more complicated numerical manipulation that is tailored to different values of l. Thus, we seek an alternative numerical approach to solve the problem. Our approach is to use the trap-free solution as the initial profile for v_s accompanied by an iterative strategy. Inspired by the approximated analytic form [19], we adopted the following parametric form to describe the normalized surface concentration:

$$v_s(\xi) = (a + \xi)^u (1 - \xi)^v \sum_{i=0}^{N} c_i P_i(\xi) \tag{17}$$

where the first and second power law terms are to address the singularity-like profiles at the cathode and anode, respectively, with the polynomial series to capture the smooth transition from the cathode to the anode. Here, u, v, and c_i are the parameters to be solved subject to the integral equations [see (13) and (16)]. For edge contact, $a = 0$ and P_i is the shifted Chebyshev polynomial [52] of the first kind for degree i defined for the interval $\xi \in [0, 1]$. For strip contact, $a = 1$ and P_i is the Chebyshev polynomial [52] of the first kind for degree i defined for the interval $\xi \in [-1, 1]$. In general, we found that $N = 3$ is good enough to reach the converged solution in a timely matter.

Note normal numerical integration schemes can fail to evaluate the singular integral in (13) and (16) due to the existence of a singularity. Thus, the singularity is extracted by using the following mathematical transformation [54]:

$$\int_a^b \frac{f(\xi')}{\xi' - \xi} d\xi' = \int_a^b \frac{f(\xi') - f(\xi)}{\xi' - \xi} d\xi' + f(\xi) \ln \frac{b - \xi}{\xi - a}. \tag{18}$$

With this transformation, standard numerical integration techniques are well suited for the evaluation. To solve (13) and (16)

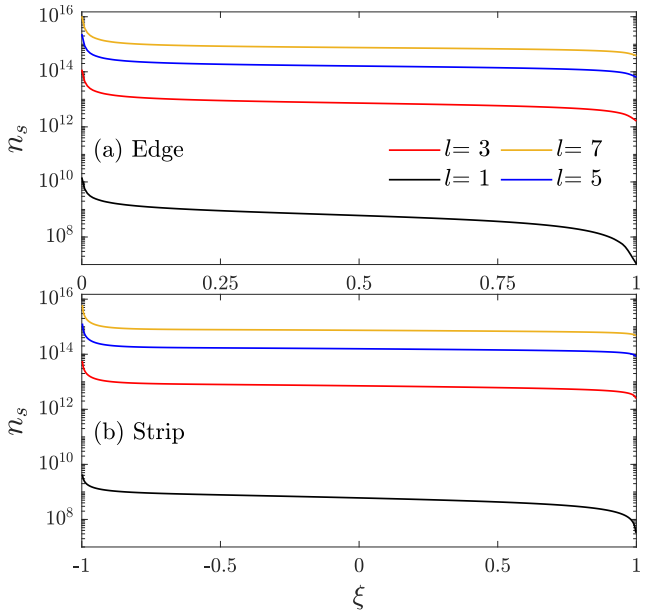

Fig. 2. Semilog profile of the calculated surface charge concentration between the cathode (left) and the anode (right) at different $l = 7$ (top) down to 1 (bottom) for (a) edge contact and (b) strip contact with the trapped-limited current of 1 μA/cm.

for different l, we first use the approximated analytic solution for trap-free cases [19] as the initial guess to calculate the solution for $l = 1$ case. The obtained solution is then used as the initial guess to solve for the next values of larger $l = l + \Delta l$. This process is iterated from $l = 1$ to $l = 10$ with a step size of $\Delta l = 0.01$ to ensure the solution of the previous iteration can be a good candidate to be used as the initial guess for the subsequent iteration. In doing so, we have implemented a numerical scheme based on the collocation method [55]. The residual errors at all the collocation points are very small, $<10^{-8}$, and generally $<10^{-3}$ elsewhere.

IV. Results and Discussions

In Fig. 2, the numerically obtained profiles (semilog plotting) of the surface charge concentration n_s at different l are plotted between the cathode (left) and anode (right) for edge contact [see Fig. 2(a)] and strip contact [see Fig. 2(b)]. The equivalent trap-free case ($l = 1$) is included for comparison. The profiles of carrier charges are similar qualitatively for both contact geometries regardless of the variation of the l. In low-dimensional systems, electron screening is strongly suppressed. As a result of easier charge carrier diffusion, the charge concentration is distributed more uniformly and drops slowly along the dielectric [15]. In contrast, the concentration is higher near the cathode and drops more rapidly near the anode. The overall magnitude of the concentration increases with l and the profile also becomes more uniform at large l.

After solving the governing equations [see (13) and (16)] of charge transport for edge and strip contact geometries, the parameter λ_l is calculated as a function of l in Fig. 3 (blue lines associated with left axis). The prefactor $(1/\lambda_l)^{l+1}$ in (4) is also plotted as a function of l in Fig. 3 (red lines associated with the right axis in log scale), which resembles a straight line. This implies that an empirical form of λ_l for both edge

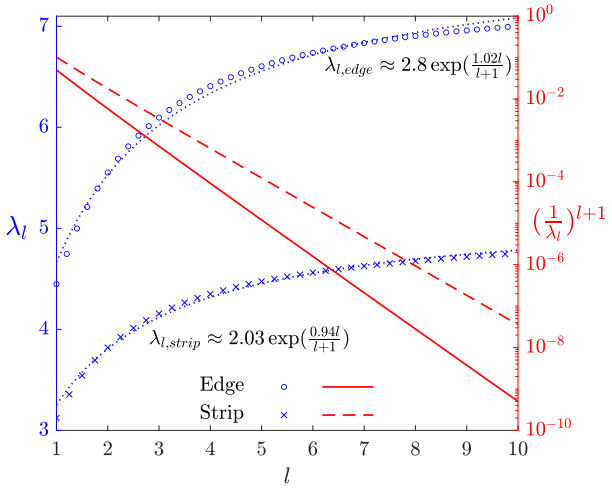

Fig. 3. Variation of the λ_l (left axis) and $\lambda_l^{-(l+1)}$ (right axis) with respect to $l = 1$ to 10 for edge contact (blue circles and red solid line) and strip contact (blue crosses and red dashed line) contact. Dotted lines are the approximated λ_l given by (19).

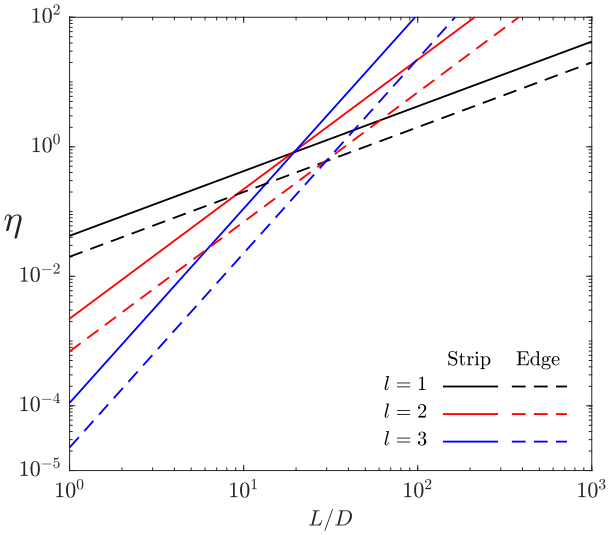

Fig. 4. Parameter $\eta = J_{2\text{-D}}/(J_{\text{MH}} \cdot D) = \mu_{\text{MH}}/\mu_{2\text{-D}}$ as a function of L/D, where $J_{2\text{-D}}$ is the line current density for 2-D ultrathin dielectrics, J_{MH} is the bulk MH current density, μ_{MH} is the MH-estimated charge mobility, $\mu_{2\text{-D}}$ is the charge mobility of 2-D ultrathin dielectrics, and L and D are the channel length and thickness, respectively.

and strip contact geometries can be assumed as

$$\lambda_l = \alpha \exp\left(\beta \frac{l}{l+1}\right) \tag{19}$$

where (α, β) are parameters determined by empirical fitting to be $(2.8, 0.94)$ and $(2.03, 1.02)$ for edge and strip contact geometries, respectively. This approximation gives a maximum relative error of $<5\%$ across the interval $l \in [1, 10]$.

From (3) and (4), both equations have the I–V scaling of $I \propto V^{l+1}$. However, the predicted carrier mobility will be substantially different. Considering a nanoscale trap-filled dielectric solid of thickness $D < L$, it is of interest to estimate the difference between the mobility estimated by (3) and (4). Assuming the current following the ultrathin dielectrics (10) equals to the current from the MG law (3), we have

$$\mathcal{J}_{2\text{-D}} \times W = J_{\text{MH}} \times W \times D. \tag{20}$$

TABLE I
$\eta = \mu_{MH}/\mu_{2\text{-D}}$ FOR L/D = 50 AND 100

l	η $(L/D = 50)$		η $(L/D = 100)$	
	Edge	Strip	Edge	Strip
2	0.35	1.09	1.42	4.36
4	0.93	6.48	14.96	103.70
6	2.56	39.32	164.04	2516.20
8	7.17	239.00	1836.32	61184.16

The ratio between the estimated carrier mobility of the MH law (μ_{MH}) to that of the ultrathin 2-D model ($\mu_{2\text{-D}}$) is

$$\eta = \frac{\mu_{MH}}{\mu_{2\text{-D}}} = \left(\frac{1}{\lambda_l}\frac{l+1}{2l+1}\right)^{l+1}\left(\frac{l+1}{2l}\right)^{l}\left(\frac{L}{D}\right)^{l}. \quad (21)$$

We plot η as a function of L/D in Fig. 4 for different values of $l = 1$, 2, and 3 with both contact types. The findings suggest that the significant difference (i.e., $\eta > 1$) will occur for large $L/D > 10$ s and the effect is more dominant for large l. For typical dielectric thin-film-based devices [4], [56], [57], [58], [59], [60], we have $L/D \gg 10$. Thus, (20) and Fig. 4 suggest that the mobility estimated using the classical bulk MH law may be problematic. In Table I, we tabulate η for $L/D =$ 50 and 100. It is observed clearly that we have $\eta > 1$ for either large l or large L/D.

Between the two contacts, strip contact will have a larger difference. Thus, under the same material properties, $\mathcal{J}_{2\text{-D}}/(J_{MH} \cdot D)$ will result in the same expression (21). Therefore, Fig. 4 also highlights that strip contact geometry will always lead to a larger current flow than edge contact geometry.

V. Conclusion

In summary, we consider a trap-filled ultrathin dielectric with exponentially distributed traps and formulate a semianalytical model to calculate the trap-limited current line density for two types of contacts, namely strip and edge contacts. The I–V scaling is found to be the same as the classical MH law (of bulk dielectrics), which is $I \propto V^{l+1}$, where l is the parameter describing the trap distribution. The dependence of the dielectric length L is, however, different, which is formulated into a trap-dependent parameter λ_l, which has an approximated analytical form. We note that the approach is general and applicable if a suitable Green's function can be identified for a configuration. The classical result of MH law can be derived by using the 1-D Green's function. In constructing the model, we have considered the vanishing limit of D and the invariance along the width direction in order to apply Green's functions. The model would be most effective in situations where D is significantly smaller than L and W is significantly larger than L. Similar findings have been reported for trap-free nanowires and thin films [15] while enhanced SCLC is reported for contacts with finite width [12], [13], [14].

Using this new model, we have discussed the possible errors in using the bulk MH law to estimate the carrier mobility for a trap-filled ultrathin dielectric with a thickness D much less than its length L (e.g., $L/D > 10$). It is found that the error is more severe for strip contact and also for large l and L/D. The strip contact geometry will always lead to larger trap-limited MH law than the edge contact geometry. Thus, this article shall offer a useful tool for quick estimation of carrier mobility of ultrathin dielectrics used in various applications such as organic electronics, 2-D materials-based electronics, and other thin-film electronics.

One distinguishing feature in our model is the different current-length scaling from the MH law. Additional experimental verification of this aspect could further validate our findings. Systematic investigation of various contact geometries could enhance our understanding of the effectiveness of the proposed model. Future improvements include the effects of the unconventional *nonparabolic* energy dispersion for 2-D materials [33] and to study the transition from the injection via Schottky contact [17].

References

[1] X.-G. Zhang and S. T. Pantelides, "Theory of space charge limited currents," *Phys. Rev. Lett.*, vol. 108, no. 26, Jun. 2012, Art. no. 266602, doi: 10.1103/PhysRevLett.108.266602.

[2] J. C. Blakesley et al., "Towards reliable charge-mobility benchmark measurements for organic semiconductors," *Org. Electron.*, vol. 15, no. 6, pp. 1263–1272, Jun. 2014, doi: 10.1016/j.orgel.2014.02.008.

[3] N. Akiyama and T. Dohi, "Space-charge-limited current with traps in trigonal selenium nanowires," *Jpn. J. Appl. Phys.*, vol. 60, no. 3, Mar. 2021, Art. no. 031003, doi: 10.35848/1347-4065/abe015.

[4] C.-Y. Jeong, H.-J. Kim, J. I. Kim, J.-H. Lee, and H.-I. Kwon, "Extraction of bulk and interface trap densities in amorphous InGaZnO thin-film transistors," *J. Vac. Sci. Technol. B, Nanotechnol. Microelectron., Mater., Process., Meas., Phenomena*, vol. 34, no. 6, Nov. 2016, Art. no. 060601, doi: 10.1116/1.4964608.

[5] P. Zhang, Y. S. Ang, A. L. Garner, A. Valfells, J. W. Luginsland, and L. K. Ang, "Space–charge limited current in nanodiodes: Ballistic, collisional, and dynamical effects," *J. Appl. Phys.*, vol. 129, no. 10, Mar. 2021, Art. no. 100902, doi: 10.1063/5.0042355.

[6] M. Sajedi Alvar, P. W. M. Blom, and G.-J.-A. H. Wetzelaer, "Space-charge-limited electron and hole currents in hybrid organic-inorganic perovskites," *Nature Commun.*, vol. 11, no. 1, p. 4023, Dec. 2020, doi: 10.1038/s41467-020-17868-0.

[7] F. Caruso, P. La Torraca, L. Larcher, G. Tallarida, and S. Spiga, "The electrons' journey in thick metal oxides," *Appl. Phys. Lett.*, vol. 121, no. 1, Jul. 2022, Art. no. 012902, doi: 10.1063/5.0097922.

[8] N. F. Mott and R. W. Gurney, *Electronic Processes in Lonic Crystals*. Oxford, U.K.: Clarendon Press, 1948.

[9] C. Child, "Discharge from hot CaO," *Phys. Rev.*, vol. 32, p. 492, May 1911, doi: 10.1103/PhysRevSeriesI.32.492.

[10] I. Langmuir, "The effect of space charge and initial velocities on the potential distribution and thermionic current between parallel plane electrodes," *Phys. Rev.*, vol. 21, no. 4, p. 419, Apr. 1923, doi: 10.1103/PhysRev.21.419.

[11] P. Zhang, Á. Valfells, L. K. Ang, J. W. Luginsland, and Y. Y. Lau, "100 years of the physics of diodes," *Appl. Phys. Rev.*, vol. 4, no. 1, Mar. 2017, Art. no. 011304, doi: 10.1063/1.4978231.

[12] W. Chandra, L. K. Ang, K. L. Pey, and C. M. Ng, "Two-dimensional analytical mott-gurney law for a trap-filled solid," *Appl. Phys. Lett.*, vol. 90, no. 15, Apr. 2007, Art. no. 153505, doi: 10.1063/1.2721382.

[13] A. A. Talin, F. Léonard, B. S. Swartzentruber, X. Wang, and S. D. Hersee, "Unusually strong space-charge-limited current in thin wires," *Phys. Rev. Lett.*, vol. 101, no. 7, Aug. 2008, Art. no. 076802, doi: 10.1103/PhysRevLett.101.076802.

[14] Y. B. Zhu and L. K. Ang, "Non-uniform space charge limited current injection into a nano contact solid," *Sci. Rep.*, vol. 5, no. 1, Mar. 2015, doi: 10.1038/srep09173.

[15] S. Alagha, A. Shik, H. E. Ruda, I. Saveliev, K. L. Kavanagh, and S. P. Watkins, "Space-charge-limited current in nanowires," *J. Appl. Phys.*, vol. 121, no. 17, May 2017, Art. no. 174301, doi: 10.1063/1.4982222.

[16] G. González, "Quantum theory of space charge limited current in solids," *J. Appl. Phys.*, vol. 117, no. 8, Feb. 2015, Art. no. 084306, doi: 10.1063/1.4913512.

[17] W. Chandra, L. K. Ang, and W. S. Koh, "Two-dimensional model of space charge limited electron injection into a diode with Schottky contact," *J. Phys. D, Appl. Phys.*, vol. 42, no. 5, Feb. 2009, Art. no. 055504.

[18] Y. B. Zhu and L. K. Ang, "Analytical re-derivation of space charge limited current in solids using capacitor model," *J. Appl. Phys.*, vol. 110, no. 9, Nov. 2011, Art. no. 094514, doi: 10.1063/1.3658811.

[19] A. Grinberg, S. Luryi, M. R. Pinto, and N. L. Schryer, "Space-charge-limited current in a film," *IEEE Trans. Electron Devices*, vol. 36, no. 6, pp. 1162–1170, Jun. 1989, doi: 10.1109/16.24363.

[20] S. Li, D. Min, W. Wang, and G. Chen, "Linking traps to dielectric breakdown through charge dynamics for polymer nanocomposites," *IEEE Trans. Dielectr. Electr. Insul.*, vol. 23, no. 5, pp. 2777–2785, Oct. 2016, doi: 10.1109/TDEI.2016.7736837.

[21] J. Dacuña, W. Xie, and A. Salleo, "Estimation of the spatial distribution of traps using space-charge-limited current measurements in an organic single crystal," *Phys. Rev. B, Condens. Matter*, vol. 86, no. 11, Sep. 2012, Art. no. 115202, doi: 10.1103/PhysRevB.86.115202.

[22] H. T. Nicolai, M. M. Mandoc, and P. W. M. Blom, "Electron traps in semiconducting polymers: Exponential versus Gaussian trap distribution," *Phys. Rev. B, Condens. Matter*, vol. 83, no. 19, May 2011, Art. no. 195204, doi: 10.1103/PhysRevB.83.195204.

[23] H. T. Nicolai et al., "Unification of trap-limited electron transport in semiconducting polymers," *Nature Mater.*, vol. 11, no. 10, pp. 882–887, Oct. 2012, doi: 10.1038/nmat3384.

[24] Y. Niu et al., "Significantly enhancing the discharge efficiency of sandwich-structured polymer dielectrics at elevated temperature by building carrier blocking interface," *Nano Energy*, vol. 97, Jun. 2022, Art. no. 107215, doi: 10.1016/j.nanoen.2022.107215.

[25] B. J. Ree, T. Isono, and T. Satoh, "Chemically controlled volatile and nonvolatile resistive memory characteristics of novel oxygen-based polymers," *ACS Appl. Mater. Interface*, vol. 12, no. 25, pp. 28435–28445, Jun. 2020, doi: 10.1021/acsami.0c06939.

[26] F. Palumbo et al., "A review on dielectric breakdown in thin dielectrics: Silicon dioxide, high-K, and layered dielectrics," *Adv. Funct. Mater.*, vol. 30, no. 18, Apr. 2019, Art. no. 1900657, doi: 10.1002/adfm.201900657.

[27] S. Lombardo, J. H. Stathis, B. P. Linder, K. L. Pey, F. Palumbo, and C. H. Tung, "Dielectric breakdown mechanisms in gate oxides," *J. Appl. Phys.*, vol. 98, no. 12, p. 121301, 2005, doi: 10.1063/1.2147714.

[28] P. Mark and W. Helfrich, "Space-charge-limited currents in organic crystals," *J. Appl. Phys.*, vol. 33, no. 1, pp. 205–215, 1962, doi: 10.1063/1.1728487.

[29] C.-P. Kwan et al., "Space-charge limited conduction in epitaxial chromia films grown on elemental and oxide-based metallic substrates," *AIP Adv.*, vol. 9, no. 5, May 2019, Art. no. 055018, doi: 10.1063/1.5087832.

[30] H. Liu, M. Yao, W. Gao, Z. Su, and X. Yao, "Dual interfacial modification via anodizing method for achieving enhanced breakdown strength in multi-layer anodized alumina/$Sr_{0.85}Bi_{0.1}TiO_3$ films," *J. Alloys Compounds*, vol. 817, Mar. 2020, Art. no. 152783, doi: 10.1016/j.jallcom.2019.152783.

[31] K. Rasool, M. A. Rafiq, and Z. A. K. Durrani, "Tailoring transport and dielectric properties by surface passivation of silicon nanowires with polyacrylic acid/TiO_2 nanoparticles composite," *Microelectronic Eng.*, vol. 119, pp. 141–145, May 2014, doi: 10.1016/j.mee.2014.03.040.

[32] Q. Zhao, W. Sun, F. Zheng, Z. An, and Y. Zhang, "Charge mobility in biaxially oriented polypropylene films," in *Proc. IEEE 2nd Int. Conf. Dielectr. (ICD)*, Budapest, Jul. 2018, pp. 1–4, doi: 10.1109/ICD.2018.8514717.

[33] Y. S. Ang, M. Zubair, and L. K. Ang, "Relativistic space-charge-limited current for massive dirac fermions," *Phys. Rev. B, Condens. Matter*, vol. 95, no. 16, Apr. 2017, Art. no. 165409, doi: 10.1103/PhysRevB.95.165409.

[34] M. Zubair, Y. S. Ang, and L. K. Ang, "Thickness dependence of space-charge-limited current in spatially disordered organic semiconductors," *IEEE Trans. Electron Devices*, vol. 65, no. 8, pp. 3421–3429, Aug. 2018, doi: 10.1109/TED.2018.2841920.

[35] Y. Y. Illarionov et al., "Insulators for 2D nanoelectronics: The gap to bridge," *Nature Commun.*, vol. 11, no. 1, p. 3285, Jul. 2020, doi: 10.1038/s41467-020-16640-8.

[36] C. Wen et al., "Dielectric properties of ultrathin CaF_2 ionic crystals," *Adv. Mater.*, vol. 32, no. 34, Jul. 2020, Art. no. 2002525, doi: 10.1002/adma.202002525.

[37] L. Britnell et al., "Electron tunneling through ultrathin boron nitride crystalline barriers," *Nano Lett.*, vol. 12, no. 3, pp. 1707–1710, Mar. 2012, doi: 10.1021/nl3002205.

[38] S. Wang et al., "Nonvolatile van der Waals heterostructure phototransistor for encrypted optoelectronic logic circuit," *ACS Nano*, vol. 16, no. 3, pp. 4528–4535, Feb. 2022, doi: 10.1021/acsnano.1c10978.

[39] S. Liang, B. Cheng, X. Cui, and F. Miao, "Van der Waals heterostructures for high-performance device applications: Challenges and opportunities," *Adv. Mater.*, Oct. 2019, Art. no. 1903800, doi: 10.1002/adma.201903800.

[40] M. Wang et al., "Robust memristors based on layered two-dimensional materials," *Nature Electron.*, vol. 1, p. 130, Feb. 2018, doi: 10.1038/s41928-018-0021-4.

[41] A. Di Bartolomeo, "Emerging 2D materials and their van der Waals heterostructures," *Nanomaterials*, vol. 10, no. 3, p. 579, Mar. 2020, doi: 10.3390/nano10030579.

[42] D. V. Christensen et al., "2022 roadmap on neuromorphic computing and engineering," *Neuromorphic Comput. Eng.*, vol. 2, no. 2, Jun. 2022, Art. no. 022501, doi: 10.1088/2634-4386/ac4a83.

[43] M. Lanza et al., "Recommended methods to study resistive switching devices," *Adv. Electron. Mater.*, vol. 5, no. 1, Jan. 2019, Art. no. 1800143, doi: 10.1002/aelm.201800143.

[44] L. Wang, L. Wang, K.-W. Ang, A. V.-Y. Thean, and G. Liang, "A compact model for 2-D poly-MoS_2 FETs with resistive switching in postsynaptic simulation," *IEEE Trans. Electron Devices*, vol. 66, no. 9, pp. 4092–4100, Sep. 2019, doi: 10.1109/TED.2019.2931069.

[45] Z. Dong et al., "Atomically thin CBRAM enabled by 2-D materials: Scaling behaviors and performance limits," *IEEE Trans. Electron Devices*, vol. 65, no. 10, pp. 4160–4166, Oct. 2018, doi: 10.1109/TED.2018.2830328.

[46] M. Waltl et al., "Perspective of 2D integrated electronic circuits: Scientific pipe dream or disruptive technology?" *Adv. Mater.*, Apr. 2022, Art. no. 2201082, doi: 10.1002/adma.202201082.

[47] W. Cao et al., "2-D layered materials for next-generation electronics: Opportunities and challenges," *IEEE Trans. Electron Devices*, vol. 65, no. 10, pp. 4109–4121, Oct. 2018, doi: 10.1109/TED.2018.2867441.

[48] P. Sang et al., "Two-dimensional silicon atomic layer field-effect transistors: Electronic property, metal-semiconductor contact, and device performance," *IEEE Trans. Electron Devices*, vol. 69, no. 4, pp. 2173–2179, Apr. 2022, doi: 10.1109/TED.2021.3138362.

[49] A. D. Bartolomeo et al., "Asymmetric Schottky contacts in bilayer MoS_2 field effect transistors," *Adv. Funct. Mater.*, vol. 28, no. 28, May 2018, Art. no. 1800657, doi: 10.1002/adfm.201800657.

[50] A. D. Bartolomeo et al., "Electrical transport and persistent photoconductivity in monolayer MoS_2 phototransistors," *Nanotechnology*, vol. 28, no. 21, May 2017, Art. no. 214002, doi: 10.1088/1361-6528/aa6d98.

[51] F. Liu et al., "2D black phosphorus/$SrTiO_3$-based programmable photoconductive switch," *Adv. Mater.*, vol. 28, no. 35, pp. 7768–7773, Jul. 2016.

[52] J. C. Mason and D. C. Handscomb, *Chebyshev Polynomials*. London, U.K.: Chapman & Hall/CRC, 2002.

[53] Y.-S. Chan, A. C. Fannjiang, and G. H. Paulino, "Integral equations with hypersingular kernels–theory and applications to fracture mechanics," *Int. J. Eng. Sci.*, vol. 41, no. 7, pp. 683–720, Apr. 2003, doi: 10.1016/S0020-7225(02)00134-9.

[54] E. H. Bareiss and C. P. Neuman, "Singular integrals and singular integral equations with a Cauchy kernel and the method of symmetric pairing," Argonne Nat. Lab., Argonne, IL, USA, Tech. Rep. ANL-6988, 1965.

[55] L. N. Trefethen, *Spectral Methods in MATLAB*. Philadelphia, PA, USA: SIAM, 2000.

[56] Z. Dai, S. K. Yadavalli, M. Chen, A. Abbaspourtamijani, Y. Qi, and N. P. Padture, "Interfacial toughening with self-assembled monolayers enhances perovskite solar cell reliability," *Science*, vol. 372, no. 6542, pp. 618–622, May 2021, doi: 10.1126/science.abf5602.

[57] G. L. Pozzoli, L. Merces, E. Yassitepe, V. B. de Morais, D. H. S. de Camargo, and C. C. B. Bufon, "Charge transport and gradient doping in nanostructured polypyrrole films for applications in photocurrent generation," *ACS Appl. Nano Mater.*, vol. 3, no. 3, pp. 3060–3070, Mar. 2020, doi: 10.1021/acsanm.0c00523.

[58] Z. Wang, Z. Lin, M. Si, and P. D. Ye, "Characterization of interface and bulk traps in ultrathin atomic layer-deposited oxide semiconductor MOS capacitors with HfO_2/In_2O_3 gate stack by C-V and conductance method," *Frontiers Mater.*, vol. 9, p. 850451, May 2022, doi: 10.3389/fmats.2022.850451.

[59] C. Tan et al., "Recent advances in ultrathin two-dimensional nanomaterials," *Chem. Rev.*, vol. 117, pp. 6225–6331, Mar. 2017, doi: 10.1021/acs.chemrev.6b00558.

[60] D. Joung, A. Chunder, L. Zhai, and S. I. Khondaker, "Space charge limited conduction with exponential trap distribution in reduced graphene oxide sheets," *Appl. Phys. Lett.*, vol. 97, no. 9, Aug. 2010, Art. no. 093105, doi: 10.1063/1.3484956.